GOETHE UNIVERSITÄT FRANKFURT AM MAIN

Fachbereich 13 Physik
Institut für theoretische Physik,
Goethe Universität Frankfurt am Main

Bachelor Thesis

Investigation of the structure of static potential flux tubes

Charlotte Meyerdierks

Frankurt am Main
21. September 2017

Advisor and first supervisor:
Prof. Dr. Marc Wagner
Institut für theoretische Physik
Johann Wolfgang von Goethe Universität Frankfurt am Main

Second supervisor:
Prof. Dr. Owe Philipsen
Institut für theoretische Physik
Johann Wolfgang von Goethe Universität Frankfurt am Main

Selbstständigkeitserklärung

Hiermit erkläre ich, dass ich die Arbeit selbstständig und ohne Benutzung anderer als der angegebenen Quellen und Hilfsmittel verfasst habe. Alle Stellen der Arbeit, die wörtlich oder sinngemäß aus Veröffentlichungen oder aus anderen fremden Texten entnommen wurden, sind von mir als solche kenntlich gemacht worden. Ferner erkläre ich, dass die Arbeit nicht - auch nicht auszugsweise - für eine andere Prüfung verwendet wurde.

Ort, Datum: _____

Unterschrift: _____ (Charlotte Meyerdierks)

Abstract

This work aims to investigate the structure of the flux tube generated by a static quark antiquark pair. For that purpose a trial state of an infinitely heavy quark and antiquark on the lattice connected by the gauge potential using SU(2)-Yang-Mills-theory is considered. At first, the potential between quark and antiquark in the lowest energy state is computed for different distances between quark and antiquark by evaluating Wilson loops. In the second part, the structure of the chromoelectric field in the direction parallel to the quark antiquark axis in the region around the quark antiquark pair is specified. This is done by computing the product of a Wilson loop between quark and antiquark and a plaquette at the place where the chromoelectric field shall be evaluated. The determined values representing the chromoelectric field are proportional to the energy density of the chromoelectromagnetic field and thereby yield the structure of the flux tube.

Zusammenfassung

Diese Arbeit dient der Erforschung von der Struktur des Flussschlauchs, der durch ein statisches Quark-Antiquark-Paar erzeugt wird. Dazu wird ein Testzustand bestehend aus unendlich schwerem Quark und Antiquark, die durch das Eichpotential auf dem Gitter verbunden sind, unter Verwendung von SU(2)-Yang-Mills-Theorie betrachtet. Zunächst wird das Potential zwischen Quark und Antiquark im Energiegrundzustand für verschiedene Abstände analysiert, indem Wilson Loops ausgewertet werden. Im zweiten Teil wird die Struktur des chromoelektrischen Feldes in paralleler Richtung zur Quark-Antiquark-Achse in der Region um das Quark-Antiquark-Paar bestimmt. Dies wird umgesetzt durch Berechnung des Produkts eines Wilson Loops zwischen Quark und Antiquark und einer Plaquette an dem Ort, wo das chromoelektrische Feld ausgewertet werden soll. Die ermittelten Werte, die die Stärke des chromoelektrischen Feldes widerspiegeln, sind ein Maß für die Energiedichte des chromoelektromagnetischen Feldes und führen damit auf die Struktur des Flussschlauchs.

Content

1 Introduction **1**

2 Calculation of the quark antiquark potential in SU(2) Yang-Mills-theory **2**
2.1 Path integral representation 3
2.2 Energy eigenvalue representation 5

3 Calculation of the chromoelectric field in SU(2) Yang-Mills-theory **7**
3.1 Plaquette expectation value 9
3.2 Expectation value of the time ordered square of the chromoelectric field . 10
3.3 Expectation value of the square of the chromoelectric field 10
3.4 Vacuum contribution 13

4 Evaluation of Wilson loops on the lattice **14**
4.1 Value assignment on the lattice 14
4.2 Error analysis 15
4.3 Smearing of Wilson loops on the lattice 15

5 Results: Quark antiquark potential **17**

6 Results: Chromoelectric field **19**
6.1 Temporal extension of the Wilson loop 21
6.2 Chromoelectric field on the quark antiquark axis 23
6.3 Chromoelectric field beside the quark antiquark axis 25

7 Conclusion and outlook **29**

Bibliography **30**

1 Introduction

Quantum Chromodynamics is a gauge theory based on the non-abelian gauge group SU(3) describing particles with colour charge red, blue and green interacting through gluon exchange. By contrast, the SU(2) Yang-Mills-theory postulates a local invariance of the Lagrangian under SU(2) transformations and describes infinitely heavy particles with two possible colour charges. The phenomena described by SU(2) Yang-Mills-theory are similar to the ones described by SU(3) Quantum Chromodynamics. Especially, confinement can be observed in both theories. In this work physical quantities are evaluated by using lattice gauge theory, which implies that calculations are implemented by discretisation of space-time. As lattice gauge theory calculations are easier and faster to perform for SU(2) Yang-Mills-theory, the computations are done on the basis of this theory.

An exciting aspect of confinement is the formation of gluonic flux tubes between quark antiquark pairs when their separation is increased. These flux tubes are related to the linear rise of the potential between quark and antiquark with increasing distance. Correspondingly, in order to investigate the structure of flux tubes, firstly the potential between quark and antiquark and secondly the energy density of the chromoelectromagnetic field will be computed.

The chromoelectric field strength E contributes to the energy density of the chromoelectromagnetic field as $\omega \sim \frac{1}{2}(E^2 + B^2)$ with the energy density ω and the chromomagnetic field strength B. In [1] the authors studied the composition of the energy density made up of chromoelectric and chromomagnetic contributions. They observed that the chromoelectric field in parallel direction (in relation to the quark antiquark axis) is dominant whereas the vertical components' and the chromomagnetic field's ratio is negligibly small. This is why in this work the chromoelectric field in parallel direction is computed to obtain the dominating contribution to the energy density.

Already in 1990 the chromoelectric flux tube was studied on the lattice in SU(2) and SU(3) gauge theory in [2].

Continuative considerations investigating the QCD flux tube in pure gauge SU(3) and fitting the flux tube profile with Gaussian and exponential functions were done in [3], [4] and [5].

2 Calculation of the quark antiquark potential in SU(2) Yang-Mills-theory

This chapter aims to derive a formula to calculate the quark antiquark potential on the lattice.

Details concerning the following computations can be found in [6].

Consider a trial state consisting of an infinitely heavy quark at point $\vec{y}$ (generated by the operator $Q_{\beta b}(\vec{y},0)$) and an infinitely heavy antiquark at point $\vec{x}$ (generated by the operator $\overline{Q}_{\alpha a}(\vec{x},0)$) connected by the gauge potential,

$$|\Phi_{\alpha\beta}(\tau=0,\vec{x},\vec{y})\rangle = \overline{Q}_{\alpha a}(\vec{x},0)U_{ab}(\vec{x},0;\vec{y},0)Q_{\beta b}(\vec{y},0)\,|\Omega\rangle = O_{\alpha\beta}(0,\vec{x},\vec{y})\,|\Omega\rangle\,. \tag{2.1}$$

τ is the euclidean time, $\alpha,\beta \in \{0,1,2,3\}$ are the Dirac indices and $a,b \in \{1,2\}$ are the colour indices. $|\Omega\rangle$ is the vacuum state. $U_{ab}(\vec{x},\tau_1;\vec{y},\tau_2)$ are the matrix-valued link-variables, that are group elements of SU(2) and can be expressed by the gauge potential A that is a linear combination of the generators of SU(2),

$$U_{ab}(\vec{x},\tau_1;\vec{y},\tau_2) = P\left(e^{ig\int_x^y dz^\mu A_\mu(z)}\right)_{ab}. \tag{2.2}$$

P is the path ordering operator and g is the coupling constant. How the path ordering is performed can be seen by dividing the path between the space-time-points $x=(\tau_1,\vec{x}) = x_0$ and $y=(\tau_2,\vec{y}) = x_n$ into n pieces of length a (lattice spacing) which corresponds to the lattice formulation of the link variable,

$$\begin{aligned} U^{lattice}_{ab}(\vec{x},\tau_1;\vec{y},\tau_2;a) &= P\left(e^{ig\sum_{l=0}^{n-1} a^\mu A_\mu(x_l)}\right)_{ab} \\ &= \left(e^{iga^\mu A_\mu(x_0)}\right)_{aa_1}\cdot\ldots\cdot\left(e^{iga^\mu A_\mu(x_{n-1})}\right)_{a_{n-1}b} \\ &= U^{lattice}_{aa_1}(x_0,x_1;a)\cdot\ldots\cdot U^{lattice}_{a_{n-1}b}(x_{n-1},x_n;a). \end{aligned} \tag{2.3}$$

The four-vector a is defined by $a=(y-x)/n$. According to Equation (2.3), the path ordering orders the lattice link variables along the path from x to y.

If the continuum limit $a\to 0$ is performed, the lattice formulation of the link variable turns into the continuum formulation.

The correlation function between the states $|\Phi_{\alpha\beta}(0)\rangle$ and $|\Phi_{\alpha'\beta'}(\tau)\rangle$, defined by

$$\begin{aligned} &C_{\alpha'\beta'\alpha\beta}(\vec{x},\vec{y},0,\tau) \\ &\quad = \langle \Phi_{\alpha'\beta'}(\tau,\vec{x},\vec{y})|\Phi_{\alpha\beta}(0,\vec{x},\vec{y})\rangle \\ &\quad = \Big\langle \Omega | T(\overline{Q}_{\beta'a'}(\vec{y},\tau)U_{a'b'}(\vec{y},\tau;\vec{x},\tau)Q_{\alpha'b'}(\vec{x},\tau)\overline{Q}_{\alpha a}(\vec{x},0)U_{ab}(\vec{x},0;\vec{y},0)Q_{\beta b}(\vec{y},0))|\Omega\Big\rangle , \end{aligned} \tag{2.4}$$

describes the euclidean time evolution of the state. Because of the infinitely heavy quark masses the correlation function is only non vanishing if the quark and antiquark positions are the same for both states.

By considering only $\tau > 0$, the time ordering can be omitted.

2.1 Path integral representation

This correlation function (Equation (2.4)) can be written in the path integral representation,

$$C_{\alpha'\beta'\alpha\beta}(\vec{x},\vec{y},0,\tau) = \frac{1}{Z}\int DA\, DQ\, D\overline{Q}\, (\overline{Q}_{\beta'a'}(\vec{y},\tau)...Q_{\beta b}(\vec{y},0))e^{-S_{gauge}-S_Q}. \tag{2.5}$$

The expression in brackets is the same as the one in the time ordering in Equation (2.4). Z corresponds to the path integral with the expression in brackets set to one.

The euclidean action in the exponential contains the Yang-Mills gauge field interaction term

$$S_{gauge}[A] = \frac{1}{4}\int d^4x\, F^a_{\mu\nu}(A(x))F^a_{\mu\nu}(A(x)) \tag{2.6}$$

and the fermionic action for the static quark and antiquark $S_Q[Q,\overline{Q},A]$.

By plugging in the action S_Q in Equation (2.5) and performing the integration over the Grassmann variables Q and $\overline{Q}$ the following result can be found [6],

$$\begin{aligned} &C_{\alpha'\beta'\alpha\beta}(\vec{x},\vec{y},0,\tau) \\ &\quad = \frac{1}{Z}\int DA\, [S_{\alpha'\beta'b'a'}(x',y',A)S_{\beta\alpha ba}(y,x,A) - S_{\alpha'\alpha b'a}(x',x,A)S_{\beta\beta'ba'}(y,y',A)] \\ &\quad\quad U_{ab}(\vec{x},0;\vec{y},0)U_{a'b'}(\vec{y},\tau;\vec{x},\tau)e^{-S_{gauge}}. \end{aligned} \tag{2.7}$$

$S(z,z',A)$ with $z=(\tau_1,\vec{z})$ and $z'=(\tau_2,\vec{z}\,')$ is the propagator describing the propagation of the quark Q from $\vec{z}$ to $\vec{z'}$ during the euclidean time difference from τ_1 to τ_2,

$$iS(z,z',A)_{cd} = \delta^3(\vec{z}-\vec{z}\,')U_{cd}(\vec{z},\tau_1,\vec{z}\,',\tau_2) \left\{\Theta(\tau_1-\tau_2)\frac{1+\gamma_0}{2}e^{-M_Q(\tau_1-\tau_2)} + \Theta(\tau_2-\tau_1)\frac{1-\gamma_0}{2}e^{M_Q(\tau_1-\tau_2)}\right\}. \quad (2.8)$$

Inserting Equation (2.8) into Equation (2.7), $C_{\alpha'\beta'\alpha\beta}(\vec{x},\vec{y},0,\tau)$ can be rewritten to

$$\begin{aligned} &C_{\alpha'\beta'\alpha\beta}(\vec{x},\vec{y},0,\tau) \\ &\quad = (P_+)_{\alpha'\alpha}\,(P_-)_{\beta\beta'}\,e^{-2M_Q\tau} \\ &\qquad \frac{1}{Z}\int DA\, U_{ab}(\vec{x},0;\vec{y},0)U_{ba'}(\vec{y},0;\vec{y},\tau)U_{a'b'}(\vec{y},\tau;\vec{x},\tau)U_{b'a}(\vec{x},\tau;\vec{x},0)e^{-S_{gauge}}, \end{aligned} \quad (2.9)$$

with the projection operators

$$P_\pm = \frac{1\pm\gamma_0}{2}. \quad (2.10)$$

The product of the two projection operator components in Equation (2.9) is only non vanishing for four combinations of indices. This is related to the fact that in the description of infinitely heavy quarks two components of the four component Dirac spinor vanish. By combining the remaining degrees of freedom, namely quark vs. antiquark and spin up vs. spin down, four different combinations exist. To get a non-vanishing correlation function one of these combinations of indices has to be chosen.

Considering the colour indices of the product of matrix-valued link variables in Equation (2.9), one finds that it is a trace in colour space of the product of link variables along a closed path C_L. Therefore, performing the transition to the lattice produces a Wilson loop,

$$\begin{aligned} W_{C_L,a,r,\tau}[U] &= U^{lattice}_{ab}(\vec{x},0;\vec{y},0;a)U^{lattice}_{ba'}(\vec{y},0;\vec{y},\tau;a)U^{lattice}_{a'b'}(\vec{y},\tau;\vec{x},\tau;a)U^{lattice}_{b'a}(\vec{x},\tau;\vec{x},0;a) \\ &= \mathrm{Tr}\left(\prod_{l\,\in\,C_L} P\left\{U^{lattice}(l;a)\right\}\right). \end{aligned} \quad (2.11)$$

This gauge invariant quantity is illustrated in Figure (2.1). C_L is the path connecting the lattice points $(0,\vec{x})$, $(0,\vec{y})$, $(\tau,\vec{y})$, $(\tau,\vec{x})$ and $(0,\vec{x})$ with $r=|\vec{y}-\vec{x}|$ on a lattice with lattice spacing a. $l \in C_L$ are all lattice points on this path and $U^{lattice}(l;a)$ all link variables connecting the point l with the following lattice point along the path. As the product of SU(2) link variables produces a SU(2) matrix and the trace of a SU(2) matrix is real, the Wilson loop has a real value.

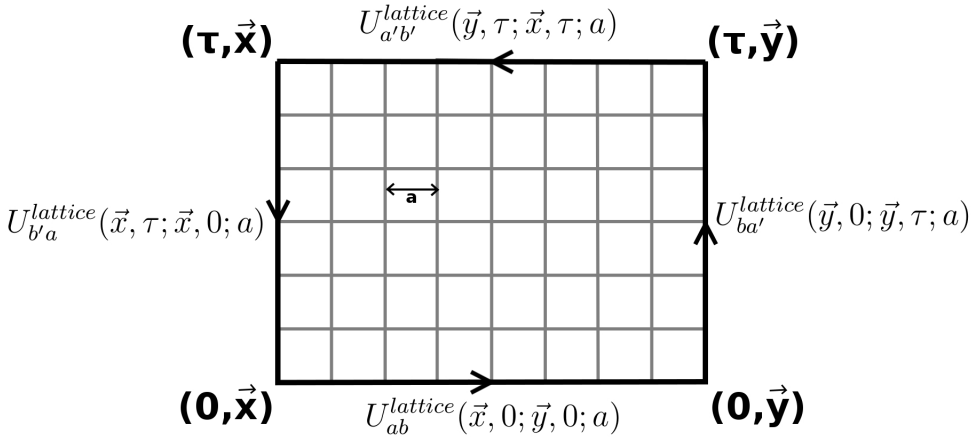

Figure 2.1: Wilson loop.

Equation (2.9) leads to the lattice expression

$$C^{lattice}_{\alpha'\beta'\alpha\beta}(\vec{x},\vec{y},0,\tau;a) = (P_+)_{\alpha'\alpha}\,(P_-)_{\beta\beta'}\,e^{-2M_Q\tau}\,\langle W_{C_L,r,\tau,a}[U]\rangle\,, \tag{2.12}$$

with

$$\lim_{a\to 0} C^{lattice}_{\alpha'\beta'\alpha\beta}(\vec{x},\vec{y},0,\tau;a) = C_{\alpha'\beta'\alpha\beta}(\vec{x},\vec{y},0,\tau;a). \tag{2.13}$$

The expression $\langle W_{C_L,r,\tau,a}[U]\rangle$ is the euclidean Wilson loop expectation value

$$\langle W_{C_L,r,\tau,a}[U]\rangle = \frac{1}{Z}\int DA\, W_{C_L,r,\tau,a}[U]e^{-S_{gauge}}. \tag{2.14}$$

2.2 Energy eigenvalue representation

The correlation function (Equation (2.4)) can also be rewritten by using the time evolution of $|\Phi_{\alpha\beta}(0,\vec{x},\vec{y})\rangle$ and inserting an identity expressed by the energy eigenbasis $|Q\overline{Q},n\rangle$,

$$C_{\alpha'\beta'\alpha\beta}(\vec{x},\vec{y},0,\tau) = \sum_n \langle\phi_{\alpha'\beta'}(0,\vec{x},\vec{y})|Q\overline{Q},n\rangle\,\langle Q\overline{Q},n|\phi_{\alpha\beta}(0,\vec{x},\vec{y})\rangle\,e^{-(E_n(r)-E_\Omega)\tau}. \tag{2.15}$$

E_Ω is the vacuum energy contribution and E_n is the energy of the n-th energy eigenstate of the system consisting of infinitely heavy quark and antiquark. By setting $\tau\to\infty$ all contributions with $n\neq 0$ vanish as they are exponentially suppressed,

$$\lim_{\tau\to\infty} C_{\alpha'\beta'\alpha\beta}(\vec{x},\vec{y},0,\tau) = \langle\phi_{\alpha'\beta'}(0,\vec{x},\vec{y})|Q\overline{Q},0\rangle\,\langle Q\overline{Q},0|\phi_{\alpha\beta}(0,\vec{x},\vec{y})\rangle\, e^{-(E_0(r)-E_\Omega)\tau}$$
$$= G_{\alpha'\beta'\alpha\beta} e^{-V_{Q\overline{Q}}(r)\tau}. \tag{2.16}$$

The state $|Q\overline{Q},0\rangle$ corresponds to the lowest energy state of the system consisting of infinitely heavy quark and antiquark and has a non-vanishing overlap with the trial state,

$$G_{\alpha'\beta'\alpha\beta} = \langle\phi_{\alpha'\beta'}(0,\vec{x},\vec{y})|Q\overline{Q},0\rangle\,\langle Q\overline{Q},0|\phi_{\alpha\beta}(0,\vec{x},\vec{y})\rangle\,. \tag{2.17}$$

In the exponent, the quark antiquark potential

$$V_{Q\overline{Q}}(r) = E_0(r) - E_\Omega \tag{2.18}$$

can be identified.

Accordingly, the quark antiquark potential can be obtained by the following expression,

$$V_{Q\overline{Q}}(r) = \lim_{\tau\to\infty} \frac{1}{a} \ln\left(\frac{C_{\alpha'\beta'\alpha\beta}(\vec{x},\vec{y},0,\tau)}{C_{\alpha'\beta'\alpha\beta}(\vec{x},\vec{y},0,\tau+a)}\right). \tag{2.19}$$

This calculation is performed on the lattice by computing the correlation functions from Wilson loops (see Equation (2.12)) leading to an expression for the effective lattice potential $V^{lattice,eff.}_{Q\overline{Q}}(r,a,\tau)$. For $a\to 0$ and $\tau\to\infty$ the lattice expression corresponds to the continuum expression $V_{Q\overline{Q}}(r)$. Consequently, the quark antiquark potential can be quantified by extrapolating lattice results for different a and τ to $a\to 0$ and $\tau\to\infty$,

$$V_{Q\overline{Q}}(r) = \lim_{a\to 0} V^{lattice}_{Q\overline{Q}}(r,a) = \lim_{\substack{\tau\to\infty\\ a\to 0}} V^{lattice,eff.}_{Q\overline{Q}}(r,a,\tau) = \lim_{\substack{\tau\to\infty\\ a\to 0}} \frac{1}{a} \ln\left(\frac{\langle|W_{C_L,r,\tau,a}[U]\rangle}{\langle W_{C_L,r,\tau+a,a}[U]\rangle}\right). \tag{2.20}$$

3 Calculation of the chromoelectric field in SU(2) Yang-Mills-theory

In the following, a formula to calculate the chromoelectric field on the lattice will be derived.

Let $P_{\mu\nu}(l,a)$ be the plaquette (the smallest Wilson loop of extension a in the directions μ and ν on a lattice with lattice spacing a) at the lattice point l,

$$\begin{aligned} P_{\mu\nu}(l,a) =& U_{ab}^{lattice}(l, l+\hat{\mu}) U_{bc}^{lattice}(l+\hat{\mu}, l+\hat{\mu}+\hat{\nu}) \\ & U_{cd}^{lattice}(l+\hat{\mu}+\hat{\nu}, l+\hat{\nu}) U_{da}^{lattice}(l+\hat{\nu}, l) \\ =& \left(e^{igaA_\mu(l)}\right)_{ab} \left(e^{igaA_\nu(l+\hat{\mu})}\right)_{bc} \left(e^{-igaA_\mu(l+\hat{\nu})}\right)_{cd} \left(e^{-igaA_\nu(l)}\right)_{da} \\ =& \mathrm{Tr}\left(e^{igaA_\mu(l)} e^{igaA_\nu(l+\hat{\mu})} e^{-igaA_\mu(l+\hat{\nu})} e^{-igaA_\nu(l)}\right). \end{aligned} \tag{3.1}$$

$\hat{\mu}$ and $\hat{\nu}$ correspond to the unit vectors of length a in the directions μ and ν, respectively.

As the plaquette can be expressed by the gluon field strength tensor, the expectation value of the field strength can be calculated by computing the expectation value of the plaquette. In order to determine the chromoelectric field, the component P_{0j} has to be evaluated. For easier computation we make use of temporal gauge $A_0 = 0$. This does not affect the value of the plaquette because it is a gauge invariant quantity. Temporal gauge leads to the expression

$$P_{0j}(l,a) = \mathrm{Tr}\left(e^{igaA_j(l+\hat{0})} e^{-igaA_j(l)}\right). \tag{3.2}$$

It is important to point out that this plaquette is a time ordered quantity, which will be used later in order to rewrite plaquette expectation values in the path integral formalism. To compute the plaquette P_{0j} the expansion of the exponential functions to order a^2 is performed,

$$e^{igaA_j(l)} = 1 + igaA_j(l) - \frac{g^2a^2}{2} A_j^2(l) + O(a^3). \tag{3.3}$$

This yields to

$$P_{0j}(l,a) = \mathrm{Tr}\left(1 + \frac{g^2a^2}{2}\left[-A_j^2(l+\hat{0}) - A_j^2(l) + 2A_j(l+\hat{0})A_j(l)\right]\right) + O(a^6). \tag{3.4}$$

Here, the property of SU(2) matrices, that the trace is always a real number, was used. Accordingly, all imaginary contributions inside Tr(...) can be omitted. This is not the case for SU(3), so that at this point the calculation is restricted to SU(2) Yang-Mills-theory.

Compare this result with the euclidean lattice formula for the field strength tensor [7],

$$E_{0j} = F_{0j} = -i\partial_0 A_j \ \rightarrow F_{0j}^{lattice}(l + \hat{0}/2) = -i\,\frac{A_j(l+\hat{0}) - A_j(l)}{a}, \tag{3.5}$$

and for the square of the field strength tensor,

$$\left[F_{0j}^{lattice}(l+\hat{0}/2)\right]^2 = \frac{1}{a^2}\left[-A_j^2(l+\hat{0}) - A_j^2(l) + A_j(l+\hat{0})A_j(l) + A_j(l)A_j(l+\hat{0})\right]. \tag{3.6}$$

If time ordering is performed in Equation (3.6), the square brackets in Equation (3.4) and (3.6) coincide, so that the time ordered square of the field strength can be expressed by the plaquette,

$$\mathrm{Tr}\left(T\left\{\left[F_{0j}^{lattice}(l+\hat{0}/2)\right]^2\right\}\right) = \frac{2}{g^2a^4}\left(P_{0j}(l,a) - 2\right) + O(a^2). \tag{3.7}$$

The time ordered square of the field strength does not correspond to the square without time ordering and therefore can not be used as a quantity representing the strength of the gluon field. Though, it is possible to find a correlation between the time ordered and not time-ordered square. Accordingly, in the next subchapters the following steps are performed in order to derive an expression for the chromoelectric field produced by the infinitely heavy quark antiquark pair (in the lowest energy state of the system consisting of quark and antiquark):

3.1) Plaquette expectation value
Evaluate the plaquette expectation value in the lowest energy state of the system consisting of infinitely heavy quark and antiquark. The plaquette is located at lattice point $l = (\vec{r}\,', 0)$,
$\langle Q\overline{Q}, 0|\, P_{0j}(\vec{r}\,', 0, a)\, |Q\overline{Q}, 0\rangle$.

3.2) Expectation value of the time ordered square of the chromoelectric field
Evaluate the expectation value of the time ordered square of the chromoelectric field in the lowest energy state of the system consisting of infinitely heavy quark and antiquark by using Equation (3.7). The chromoelectric field is calculated at lattice point $l + \hat{0}/2 = (\vec{r}\,', a/2)$,
$\langle Q\overline{Q}, 0|\, \mathrm{Tr}\left(T\left\{\left[F_{0j}^{lattice}(\vec{r}\,', a/2)\right]^2\right\}\right) |Q\overline{Q}, 0\rangle$.

3.3) Expectation value of the square of the chromoelectric field
Find the correlation between $\langle Q\overline{Q}, 0|\, \mathrm{Tr}\left(T\left\{\left[F_{0j}^{lattice}(\vec{r}\,', a/2)\right]^2\right\}\right) |Q\overline{Q}, 0\rangle$ and

$\langle Q\overline{Q}, 0| \operatorname{Tr}\left(\left[F_{0j}^{lattice}(\vec{r}\,', a/2)\right]^2\right) |Q\overline{Q}, 0\rangle$ to evaluate the expectation value of the chromoelectric field.

3.4) Vacuum contribution

To find the final result for the chromoelectric field produced by the quark antiquark pair, the vacuum contributions have to be subtracted from the expectation value in the lowest energy state,
$\langle Q\overline{Q}, 0| \operatorname{Tr}\left(\left[F_{0j}^{lattice}(\vec{r}\,', a/2)\right]^2\right) |Q\overline{Q}, 0\rangle - \langle\Omega| \operatorname{Tr}\left(\left[F_{0j}^{lattice}(\vec{r}\,', a/2)\right]^2\right) |\Omega\rangle$.

3.1 Plaquette expectation value

In order to calculate the plaquette expectation value $\langle 0| P_{0j}(\vec{r}\,', 0, a) |0\rangle$ we follow similar steps as in the derivation of the lattice formula for the quark antiquark potential. The first step is to calculate the correlation function $\langle\phi_{\alpha'\beta'}(\tau, \vec{x}, \vec{y})|P_{0j}(\vec{r}\,', \tau/2, a)|\phi_{\alpha\beta}(0, \vec{x}, \vec{y})\rangle$. To use the path integral representation, the argument between $\langle\Omega|$ and $|\Omega\rangle$ has to be time-ordered, which is fulfilled by the given argument,

$$\begin{aligned}&\langle\phi_{\alpha'\beta'}(\tau, \vec{x}, \vec{y})|P_{0j}(\vec{r}\,', \tau/2, a)|\phi_{\alpha\beta}(0, \vec{x}, \vec{y})\rangle \\ &\quad= \frac{1}{Z}\int DA\, DQ\, D\overline{Q}\, (O^\dagger(\tau))_{\alpha'\beta'} P_{0j}(\vec{r}\,', \tau/2, a)(O(0))_{\alpha\beta} e^{-S_{gauge}-S_Q}. \end{aligned} \tag{3.8}$$

The additional factor $P_{0j}(\vec{r}\,', \tau/2, a)$ does not affect the calculation we did in the derivation of Equation (2.12). So we can rewrite Equation (3.8) to

$$\begin{aligned}&\lim_{\substack{\tau\to\infty\\ a\to 0}} \langle\phi_{\alpha'\beta'}(\tau, \vec{x}, \vec{y})|P_{0j}(\vec{r}\,', \tau/2, a)|\phi_{\alpha\beta}(0, \vec{x}, \vec{y})\rangle \\ &\qquad= \lim_{\substack{\tau\to\infty\\ a\to 0}} (P_+)_{\alpha'\alpha}(P_-)_{\beta\beta'} e^{-2M_Q\tau} \left\langle W_{C_{L,r,\tau,a}}[U] P_{0j}(\vec{r}\,', \tau/2, a)\right\rangle. \end{aligned} \tag{3.9}$$

The energy eigenvalue representation is a second possibility to rewrite the correlation function $\langle\phi_{\alpha'\beta'}(\tau, \vec{x}, \vec{y})|P_{0j}(\vec{r}\,', \tau/2, a)|\phi_{\alpha\beta}(0, \vec{x}, \vec{y})\rangle$. Replacing the time dependent operators by the euclidean time evolution of the operators at time $\tau = 0$ and inserting twice an identity expressed by the energy eigenbases $\langle Q\overline{Q}, n|$ and $\langle Q\overline{Q}, m|$ leads to

$$\begin{aligned}&\langle\phi_{\alpha'\beta'}(\tau, \vec{x}, \vec{y})|P_{0j}(\vec{r}\,', \tau/2, a)|\phi_{\alpha\beta}(0, \vec{x}, \vec{y})\rangle \\ &\quad= \sum_{n,m} \langle\phi_{\alpha'\beta'}(0, \vec{x}, \vec{y})|Q\overline{Q}, n\rangle \langle Q\overline{Q}, n| P_{0j}(\vec{r}\,', 0, a) |Q\overline{Q}, m\rangle \langle Q\overline{Q}, m|\phi_{\alpha\beta}(0, \vec{x}, \vec{y})\rangle \\ &\qquad e^{-\left(\frac{1}{2}E_m(r)+\frac{1}{2}E_n(r)-E_\Omega\right)\tau}. \end{aligned} \tag{3.10}$$

By setting $\tau \to \infty$ all contributions with $n \neq 0$ or $m \neq 0$ vanish as they are exponentially suppressed. Comparing the result with the calculation in Equation (2.16) and (2.12) yields

$$\begin{aligned}
&\lim_{\substack{\tau\to\infty\\ a\to 0}} \langle \phi_{\alpha'\beta'}(\tau,\vec{x},\vec{y})|P_{0j}(\vec{r}\,',\tau/2,a)|\phi_{\alpha\beta}(0,\vec{x},\vec{y})\rangle \\
&\quad = \lim_{a\to 0} \langle \phi_{\alpha'\beta'}(0,\vec{x},\vec{y})|_{Q\overline{Q}},0\rangle \langle_{Q\overline{Q}},0|\phi_{\alpha\beta}(0,\vec{x},\vec{y})\rangle\, e^{-(E_0(r)-E_\Omega)\tau} \langle_{Q\overline{Q}},0|\, P_{0j}(\vec{r}\,',0,a)\,|_{Q\overline{Q}},0\rangle \\
&\quad = \lim_{\substack{\tau\to\infty\\ a\to 0}} C_{\alpha'\beta'\alpha\beta}(\vec{x},\vec{y},0,\tau)\, \langle_{Q\overline{Q}},0|\, P_{0j}(\vec{r}\,',0,a)\,|_{Q\overline{Q}},0\rangle \qquad (3.11) \\
&\quad = \lim_{\substack{\tau\to\infty\\ a\to 0}} (P_+)_{\alpha'\alpha}(P_-)_{\beta\beta'} e^{-2M_Q\tau} \left\langle W_{C_{L,r,\tau,a}}[U]\right\rangle \langle_{Q\overline{Q}},0|\, P_{0j}(\vec{r}\,',0,a)\,|_{Q\overline{Q}},0\rangle\,. \qquad (3.12)
\end{aligned}$$

By comparing the path integral representation in Equation (3.9) and the energy eigenvalue representation in Equation (3.12) we find an expression to calculate $\langle_{Q\overline{Q}},0|\, P_{0j}(\vec{r}\,',0)\,|_{Q\overline{Q}},0\rangle$ on the lattice,

$$\lim_{a\to 0} \langle_{Q\overline{Q}},0|\, P_{0j}(\vec{r}\,',0,a)\,|_{Q\overline{Q}},0\rangle = \lim_{\substack{\tau\to\infty\\ a\to 0}} \frac{\left\langle W_{C_{L,r,\tau,a}}[U] P_{0j}(\vec{r}\,',\tau/2,a)\right\rangle}{\left\langle W_{C_{L,r,\tau,a}}[U]\right\rangle}. \qquad (3.13)$$

3.2 Expectation value of the time ordered square of the chromoelectric field

By using Equation (3.7) and (3.13) we get the following result for the expectation value of the time ordered square of the chromoelectric field,

$$\begin{aligned}
&\lim_{a\to 0} \langle_{Q\overline{Q}},0|\,\mathrm{Tr}\left(T\left\{\left[F_{0j}^{lattice}(\vec{r}\,',a/2)\right]^2\right\}\right)|_{Q\overline{Q}},0\rangle \\
&\quad = \lim_{a\to 0} \frac{2}{g^2a^4}\left(\langle_{Q\overline{Q}},0|\, P_{0j}(\vec{r}\,',0,a)\,|_{Q\overline{Q}},0\rangle - 2\right) \\
&\quad = \lim_{\substack{\tau\to\infty\\ a\to 0}} \frac{2}{g^2a^4}\left(\frac{\left\langle W_{C_{L,r,\tau,a}}[U] P_{0j}(\vec{r}\,',\tau/2,a)\right\rangle}{\left\langle W_{C_{L,r,\tau,a}}[U]\right\rangle} - 2\right). \qquad (3.14)
\end{aligned}$$

3.3 Expectation value of the square of the chromoelectric field

This subchapter aims to find the relation between the lowest energy state expectation value of the time ordered square of the chromoelectric field and the square of the chromoelectric field without time ordering.

The same calculation that led to Equation (3.11) provides the following two equations,

$$\lim_{\tau\to\infty} \langle\phi_{\alpha'\beta'}(\tau,\vec{x},\vec{y})|\,\mathrm{Tr}\left(\left[F_{0j}^{lattice}(\vec{r}\,',\tau/2+a/2)\right]^2\right)|\phi_{\alpha\beta}(0,\vec{x},\vec{y})\rangle$$
$$= \lim_{\tau\to\infty} C_{\alpha'\beta'\alpha\beta}(\vec{x},\vec{y},0,\tau)\,\langle Q\overline{Q},0|\,\mathrm{Tr}\left(\left[F_{0j}^{lattice}(\vec{r}\,',a/2)\right]^2\right)|Q\overline{Q},0\rangle\,, \tag{3.15}$$

$$\lim_{\tau\to\infty} \langle\phi_{\alpha'\beta'}(\tau,\vec{x},\vec{y})|\,\mathrm{Tr}\left(T\left\{\left[F_{0j}^{lattice}(\vec{r}\,',\tau/2+a/2)\right]^2\right\}\right)|\phi_{\alpha\beta}(0,\vec{x},\vec{y})\rangle$$
$$= \lim_{\tau\to\infty} C_{\alpha'\beta'\alpha\beta}(\vec{x},\vec{y},0,\tau)\,\langle Q\overline{Q},0|\,\mathrm{Tr}\left(T\left\{\left[F_{0j}^{lattice}(\vec{r}\,',a/2)\right]^2\right\}\right)|Q\overline{Q},0\rangle\,. \tag{3.16}$$

In consideration of these equations it becomes obvious that the function of interest can be found by determination of the correlation between the two trial state expectation values. To achieve that, the following computation is performed. The same calculation for quantum mechanics can be found in [6].

Let l'' be a lattice point with the same spacial coordinates but a different time coordinate τ'' in comparison to the lattice point l' with time coordinate τ'. Suppose that τ' and τ'' both are $\in [0,\tau]$. Differentiating the expression

$$\frac{1}{Z}\int DA\,DQ\,D\overline{Q}\,\left(O_{\alpha\beta}^{\dagger}(\tau,\vec{x},\vec{y})\mathrm{Tr}\left(A_j(l')A_j(l'')\right)O_{\alpha\beta}(0,\vec{x},\vec{y})\right)e^{-S_{gauge}-S_Q}$$
$$= \langle\phi_{\alpha'\beta'}(\tau,\vec{x},\vec{y})|\,\mathrm{Tr}\left(T\left\{A_j(l')A_j(l'')\right\}\right)|\phi_{\alpha\beta}(0,\vec{x},\vec{y})\rangle$$
$$= \langle\phi_{\alpha'\beta'}(\tau,\vec{x},\vec{y})|\,\mathrm{Tr}\left(\theta(\tau'-\tau'')A_j(l')A_j(l'')+\theta(\tau''-\tau')A_j(l'')A_j(l')\right)|\phi_{\alpha\beta}(0,\vec{x},\vec{y})\rangle \tag{3.17}$$

two times with respect to τ' and τ'' (in lattice formulation) leads to a definition of the difference between the two trial state expectation values in Equation (3.15) and Equation (3.16).

Differentiation with respect to τ' yields

$$\frac{1}{Z}\int DA\,DQ\,D\overline{Q}\,\left(O_{\alpha\beta}^{\dagger}(\tau,\vec{x},\vec{y})\mathrm{Tr}\left(-iF_{0j}^{lattice}(l')A_j(l'')\right)O_{\alpha\beta}(0,\vec{x},\vec{y})\right)e^{-S_{gauge}-S_Q}$$
$$= \langle\phi_{\alpha'\beta'}(\tau,\vec{x},\vec{y})|\,\mathrm{Tr}\left(-i\theta(\tau'-\tau'')F_{0j}^{lattice}(l')A_j(l'')-i\theta(\tau''-\tau')A_j(l'')F_{0j}^{lattice}(l')\right)$$
$$|\phi_{\alpha\beta}(0,\vec{x},\vec{y})\rangle\,. \tag{3.18}$$

The two terms containing delta-functions produced by the differentiation of the two theta-functions cancel each other due to different signs.

Differentiation with respect to τ'' yields

$$\frac{1}{Z}\int DA\,DQ\,D\overline{Q}\,\left(O_{\alpha\beta}^{\dagger}(\tau,\vec{x},\vec{y})\mathrm{Tr}\left(-F_{0j}^{lattice}(l')F_{0j}^{lattice}(l'')\right)O_{\alpha\beta}(0,\vec{x},\vec{y})\right)e^{-S_{gauge}-S_Q}$$
$$= \langle\phi_{\alpha'\beta'}(\tau,\vec{x},\vec{y})|\,\mathrm{Tr}\left(-i\delta(\tau'-\tau'')\left[A_j(l''),F_{0j}^{lattice}(l')\right]-T'\left\{F_{0j}^{lattice}(l')F_{0j}^{lattice}(l'')\right\}\right)$$
$$|\phi_{\alpha\beta}(0,\vec{x},\vec{y})\rangle\,. \tag{3.19}$$

It must be pointed out that the time-ordering appearing in Equation (3.14) on the left hand side and in Equation (3.19) do not coincide. The time-ordering in Equation (3.14) denoted by $T\{...\}$ time-orders all products of A_j appearing in the quadration of $F_{0j}^{lattice}(l')$. In contrast, the time ordering in Equation (3.19) denoted by $T'\{...\}$ time-orders only the fixed $F_{0j}^{lattice}(l')$ and $F_{0j}^{lattice}(l'')$ depending on τ' and τ'',

$$T'\left\{F_{0j}^{lattice}(l')F_{0j}^{lattice}(l'')\right\} = \theta(\tau'-\tau'')F_{0j}^{lattice}(l')F_{0j}^{lattice}(l'')+ \\ \theta(\tau''-\tau')F_{0j}^{lattice}(l'')F_{0j}^{lattice}(l'). \tag{3.20}$$

The time-ordering in Equation (3.19) is fulfilled by definition because the Hamiltonian of the system does only depend on $F_{0j}^{lattice}(l')$, so that it commutes with $F_{0j}^{lattice}(l')$. Consequently, $F_{0j}^{lattice}(l')$ and $F_{0j}^{lattice}(l'')$ commute. Accordingly, the time-ordering operator $T'\{...\}$ can be omitted.

On a lattice with lattice spacing a the delta function in Equation (3.19) merges to

$$\delta(\tau'-\tau'') \to \frac{1}{a}\delta_{l'l''} = \int_{-\pi/a}^{\pi/a}\frac{dA}{2\pi}e^{iA(l'-l'')a}, \tag{3.21}$$

$$\delta(0) \to \frac{1}{a}\delta_{l'l'} = \int_{-\pi/a}^{\pi/a}\frac{dA}{2\pi} = \frac{1}{a}. \tag{3.22}$$

The path integral in Equation (3.19) can be rewritten to the vacuum expectation value of the expression appearing inside the path integral by writing that expression in time-ordered products of A_j. This is exactly what the time ordering $T\{...\}$ does,

$$\frac{1}{Z}\int DA\,DQ\,D\overline{Q}\,\left(O_{\alpha\beta}^{\dagger}(\tau,\vec{x},\vec{y})\mathrm{Tr}\left(F_{0j}^{lattice}(l')F_{0j}^{lattice}(l'')\right)O_{\alpha\beta}(0,\vec{x},\vec{y})\right)e^{-S_{gauge}-S_Q} \\ = \langle\phi_{\alpha'\beta'}(\tau,\vec{x},\vec{y})|\,\mathrm{Tr}\left(T\left\{F_{0j}^{lattice}(l')F_{0j}^{lattice}(l'')\right\}\right)|\phi_{\alpha\beta}(0,\vec{x},\vec{y})\rangle\,. \tag{3.23}$$

The commutator in Equation (3.19) has the value

$$\left[A_j(l''),F_{0j}^{lattice}(l')\right] = i\delta_{l''l'}. \tag{3.24}$$

Considering Equation (3.19) for $\tau' = \tau'' = \tau/2 + a/2$ and spacial coordinate $\vec{r}\,'$ the following result can be found,

$$\langle\phi_{\alpha'\beta'}(\tau,\vec{x},\vec{y})|\,\mathrm{Tr}\left(\left[F_{0j}^{lattice}(\vec{r}\,',\tau/2+a/2)\right]^2\right)|\phi_{\alpha\beta}(0,\vec{x},\vec{y})\rangle \\ = \frac{2}{a}\,C_{\alpha'\beta'\alpha\beta}(\vec{x},\vec{y},0,\tau)+ \\ \langle\phi_{\alpha'\beta'}(\tau,\vec{x},\vec{y})|\,\mathrm{Tr}\left(T\left\{\left[F_{0j}^{lattice}(\vec{r}\,',\tau/2+a/2)\right]^2\right\}\right)|\phi_{\alpha\beta}(0,\vec{x},\vec{y})\rangle\,. \tag{3.25}$$

In combination with Equation (3.15) and (3.16) this equation has the outcome

$$\langle Q\overline{Q},0|\,\mathrm{Tr}\left(\left[F_{0j}^{lattice}(\vec{r}\,',a/2)\right]^2\right)|Q\overline{Q},0\rangle=\frac{2}{a}+\langle Q\overline{Q},0|\,\mathrm{Tr}\left(T\left\{\left[F_{0j}^{lattice}(\vec{r}\,',a/2)\right]^2\right\}\right)|Q\overline{Q},0\rangle\,. \tag{3.26}$$

3.4 Vacuum contribution

For the vacuum contribution a similar calculation as in the previous chapter is performed. Starting with the expression on the left hand side of Equation (3.17) dropping $O^{\dagger}_{\alpha\beta}(\tau,\vec{x},\vec{y})$ and $O_{\alpha\beta}(0,\vec{x},\vec{y})$ yields

$$\langle\Omega|\,\mathrm{Tr}\left(\left[F_{0j}^{lattice}(\vec{r}\,',a/2)\right]^2\right)|\Omega\rangle=\frac{2}{a}+\langle\Omega|\,\mathrm{Tr}\left(T\left\{\left[F_{0j}^{lattice}(\vec{r}\,',a/2)\right]^2\right\}\right)|\Omega\rangle\,. \tag{3.27}$$

In addition, Equation (3.7) gives

$$\langle\Omega|\,\mathrm{Tr}\left(T\left\{\left[F_{0j}^{lattice}(\vec{r}\,',a/2))\right]^2\right\}\right)|\Omega\rangle=\langle\Omega|\,\frac{2}{g^2a^4}\left(P_{0j}(\vec{r}\,',0,a)-2\right)|\Omega\rangle+O(a^2). \tag{3.28}$$

In temporal gauge the plaquette is a time ordered quantity. This is why the vacuum expectation value and the expectation value that is calculated on the lattice are the same,

$$\langle\Omega|\,P_{0j}(\vec{r}\,',0,a)\,|\Omega\rangle=\frac{1}{Z}\int DA\,P_{0j}(\vec{r}\,',0,a)e^{-S_{gauge}}=\langle P_{0j}(\vec{r}\,',0,a)\rangle\,. \tag{3.29}$$

Considering the results in Equation (3.14), (3.26), (3.27), (3.28) and (3.29) we get the final result to compute the chromoelectric field on the lattice,

$$\begin{aligned}
&\langle Q\overline{Q},0|\,\mathrm{Tr}\left([E_j(\vec{r}\,')]^2\right)|Q\overline{Q},0\rangle-\langle\Omega|\,\mathrm{Tr}\left([E_j(\vec{r}\,')]^2\right)|\Omega\rangle\\
&\quad=\lim_{a\to0}\left\{\langle Q\overline{Q},0|\,\mathrm{Tr}\left(\left[F_{0j}^{lattice}(\vec{r}\,',a/2)\right]^2\right)|Q\overline{Q},0\rangle-\langle\Omega|\,\mathrm{Tr}\left(\left[F_{0j}^{lattice}(\vec{r}\,',a/2)\right]^2\right)|\Omega\rangle\right\}\\
&\quad=\lim_{\substack{\tau\to\infty\\a\to0}}\frac{2}{g^2a^4}\left\{\frac{\left\langle W_{C_{L,r,\tau,a}}[U]P_{0j}(\vec{r}\,',\tau/2,a)\right\rangle}{\left\langle W_{C_{L,r,\tau,a}}[U]\right\rangle}-\langle P_{0j}(\vec{r}\,',0,a)\rangle\right\}.
\end{aligned} \tag{3.30}$$

4 Evaluation of Wilson loops on the lattice

As discussed in the previous chapters, the two quantities that will be evaluated (the quark antiquark potential and the chromoelectric field) are assigned to expectation values of Wilson loops and plaquettes, which are Wilson loops as well. Consequently, Wilson loops are the quantities to calculate on the lattice.

4.1 Value assignment on the lattice

In order to compute Wilson loops and plaquettes on the lattice, every lattice point l has to be assigned to link variables $U_{ab}^{lattice}(l, l+\hat{\mu})$. Accordingly, every lattice point is attached to four SU(2) matrices describing the links in three spacial and one temporal direction. The values of these matrices represent the strength of the gauge potential. Corresponding to quantum field theoretical considerations all configurations of a link variable and therefore all values of these matrices contribute to measurable quantities. Every configuration of a link variable contributes to measurements weighted by the action that results from this configuration. This is why an algorithm producing configurations of link variables weighted by the action is needed, so that the gauge field configuration of the whole lattice can be generated from this amount of link variables. For this work a given program [8] producing gauge field configurations using the **heatbath algorithm** [6] is applied.

Before the heatbath algorithm can be used, the SU(2) matrices have to be initialised with starting values. Either a cold start with all SU(2) matrices set to the unit matrix or a hot start with all SU(2) matrices chosen randomly is possible. The heatbath algorithm produces new lattice configurations by changing only a single link of the previous configuration at a time according to the distribution $e^{-S_{gauge}}$, where all other links are fixed. After an amount of thermalisation steps the lattice gauge field configuration reaches a status, where every link variable configuration appears weighted by its action, so that averaging over the whole lattice produces realistic results. As can be seen in Figure 4.1, after about 100 thermalisation steps the expectation value of the plaquette for cold and hot start coincide. Since generating gauge field configurations does not take much computing time, configuration numbers starting from 300 are used to have assurance that the thermalisation is completed.

In order to generate accurate results, an infinite lattice would be needed. Instead, a lattice with a fixed temporal and spacial extension that repeats periodically is used. To improve the results, after firstly averaging over the results generated on different lattice points of a gauge field configuration, a second averaging over different gauge field configurations is performed.

In the heatbath algorithm the parameter seed can be chosen. Using the same value of seed in a new process of producing lattice gauge field configurations the same configurations will be produced again. The parameter β is a value defining the lattice spacing a. The relation between β and a has to be determined by computing a physical quantity, e.g. the string tension, in lattice units and identifying the result with the corresponding experimental result. Here, the relations between particular a and β, published in [9] and achieved by identifying r_0 with 0.46fm in the equation $|F_{Q\overline{Q}}(r_0)r_0^2| = 1.65$, are used.

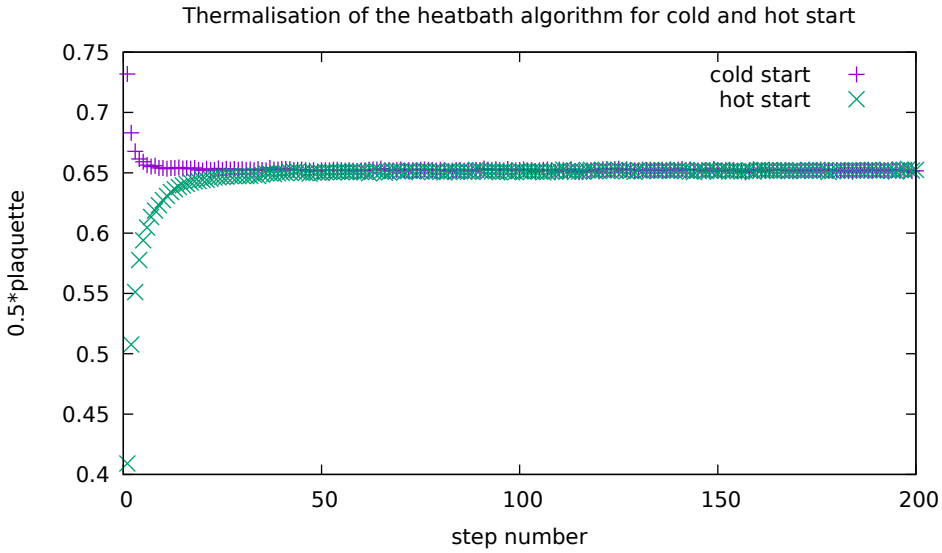

Figure 4.1: Plaquette expectation value generated by averaging over the whole lattice and all possible directions with lattice configuration depending on the step number of the heatbath algorithm.
Lattice parameters: $\beta = 2.5 \Rightarrow a = 0.073$ fm, temporal and spacial extension of the lattice $T = L = 18$.

4.2 Error analysis

Because of the functionality of the heatbath algorithm, configurations generated consecutively and therefore quantities calculated using these configurations are correlated. So it is reasonable not to use configurations appearing consecutively but to use configurations with more steps of the algorithm lying between them. In this work every hundredth configuration is used.

To take into consideration that the formulas for the static quark antiquark potential and the chromoelectric field are functions of expectation values containing quotients and logarithms, the error analysis is performed using the Jackknife error [10].

4.3 Smearing of Wilson loops on the lattice

As the trial state $|\phi_{\alpha\beta}(0, \vec{x}, \vec{y})\rangle$ and the lowest energy eigenstate $|Q\overline{Q}, 0\rangle$ of the system consisting of infinitely heavy quark and antiquark do not coincide, the limit $\tau \to \infty$

has to be taken in the calculation of the potential (see Equation (2.15) and (2.20)). The more similar these two states are, the lower τ can be chosen to achieve that only the state $|Q\overline{Q}, 0\rangle$ contributes in Equation (2.15). Choosing a low value of τ is helpful in numerical calculations because the relative error decreases with decreasing τ (see Equation (2.16): The correlation function and consequently the absolute value of the Wilson loop increases with decreasing τ so that the relative error of the Wilson loop decreases). The similarity between the two states can be increased by using **APE smearing** (cf. [11] and references therein). Whereas in a normal Wilson loop only link variables along the axis between quark and antiquark are multiplied, it is known that the strong interaction between quark and antiquark is characterised by a flux tube having a non vanishing cross-sectional area. Accordingly, the trial state can be aligned with the lowest energy eigenstate $|Q\overline{Q}, 0\rangle$ by expanding every link variable on the axis by link variables following a path that leaves the axis on a spacial lattice piece vertical to the axis, follows a path that is parallel to the axis for one lattice piece and returns back to the axis. This can be done in four directions around the axis. In comparison to the link on the axis the four ears of links are weighted by the APE smearing parameter α. This procedure of smearing all spacial links is performed N_{APE} times. Summing up, APE smearing stretches out the spacial part of Wilson loops from a line to kind of a flux tube between quark and antiquark.

Another possibility to decrease the relative error of the Wilson loops is to use a different lattice discretisation of the static quarks, the **HYP2** static action [12]. This results in a smearing of the temporal links of the Wilson loops. For small distances of the quarks this produces systematical errors but for larger separations it is a helpful concept to improve the accuracy of the results. Due to Heisenberg's uncertainty relation a fixed temporal link effects an infinitely wide momentum distribution, so that also infinitely high momenta contribute. A smearing of the temporal links makes sense in order to reduce the value of the highest momentum contribution. The lower the momentum the smaller the value of the potential which affects the relative error of the Wilson loop in the same way as the decreasing of τ does (see Equation (2.16)).

5 Results: Quark antiquark potential

Following Equation (2.20), for evaluating the effective lattice potential $V_{Q\overline{Q}}^{lattice,eff.}(r,a,\tau)$ between a quark and an antiquark separated by r, Wilson loops with spacial extension r and different temporal extensions τ and $\tau + a$ have to be calculated,

$$V_{Q\overline{Q}}(r) = \lim_{a\to 0} V_{Q\overline{Q}}^{lattice}(r,a) = \lim_{\substack{\tau\to\infty \\ a\to 0}} V_{Q\overline{Q}}^{lattice,eff.}(r,a,\tau) = \lim_{\substack{\tau\to\infty \\ a\to 0}} \frac{1}{a} \ln\left(\frac{\langle |W_{C_L,r,\tau,a}[U]\rangle}{\langle W_{C_L,r,\tau+a,a}[U]\rangle}\right). \tag{5.1}$$

For fixed r, a and τ the value of the effective lattice potential is generated by averaging the value of a Wilson loop with temporal extension τ and the value of a Wilson loop with temporal extension $\tau + a$ over the three possible spacial directions on every lattice point of each configuration, respectively. Afterwards the logarithm of the quotient is calculated and divided by the lattice spacing. The outcome of this is Figure 5.1 in which the lattice potential depending on the time extension τ is plotted for different quark antiquark separations r.

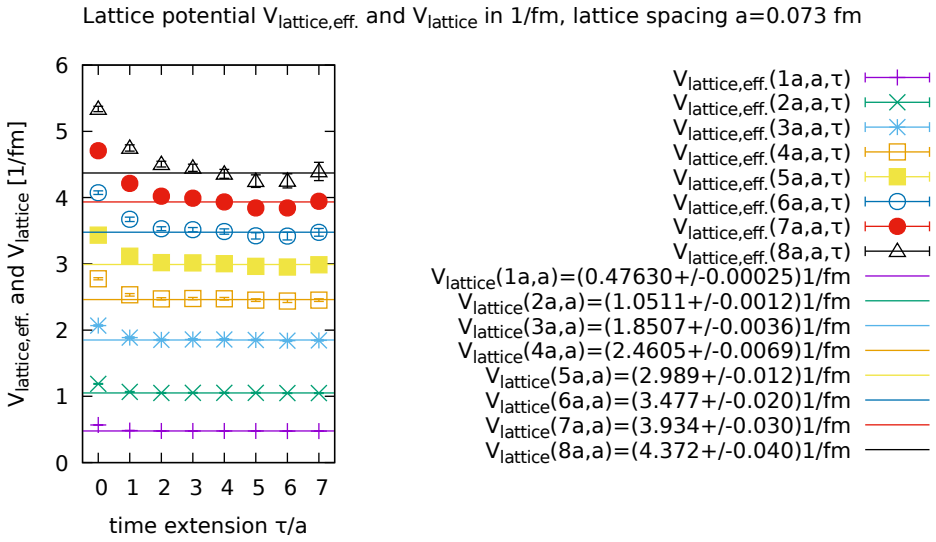

Figure 5.1: Effective lattice potential $V_{Q\overline{Q}}^{lattice,eff.}(r,a,\tau)$ and lattice potential $V_{Q\overline{Q}}^{lattice}(r,a)$.
Lattice parameters: $\beta = 2.5 \Rightarrow a = 0.073$ fm, temporal and spacial extension of the lattice $T = L = 18$, hot start, 3200 configurations produced of which 30 configurations $\{300, 400, ..., 3200\}$ are used.
APE smearing parameters for the Wilson loops: $N_{APE} = 15$, $\alpha = 0.5$.
The error bars for the values of $V_{Q\overline{Q}}^{lattice,eff.}(r,a,\tau)$ are Jackknife errors whereas the errors of $V_{Q\overline{Q}}^{lattice}(r,a)$ are the errors of the linear fit of the lattice potential for $\hat{\tau} = \{3, ..., 7\}$ taking the Jackknife errors into account.

As APE smearing and HYP2 smearing is used in the computation of the Wilson loops, the result for $V_{Q\overline{Q}}^{lattice,eff.}(r,a,\tau)$ converges already for values of τ in the range $\hat{\tau} = \tau/a \in \{3,..,7\}$ and not only for $\tau \to \infty$. Accordingly, the potential $V_{Q\overline{Q}}^{lattice}(r,a)$ is computed for fixed r and a by averaging $V_{Q\overline{Q}}^{lattice,eff.}(r,a,\tau)$ for $\hat{\tau} \in \{3,...,7\}$.

By doing the same calculation for gauge coupling $\beta = 2.4$ corresponding to lattice spacing $a = 0.102$ fm, in Figure 5.2 the values of $V_{Q\overline{Q}}^{lattice}(r,a)$ as a function of the distance r between quark and antiquark are plotted for both lattice spacings.

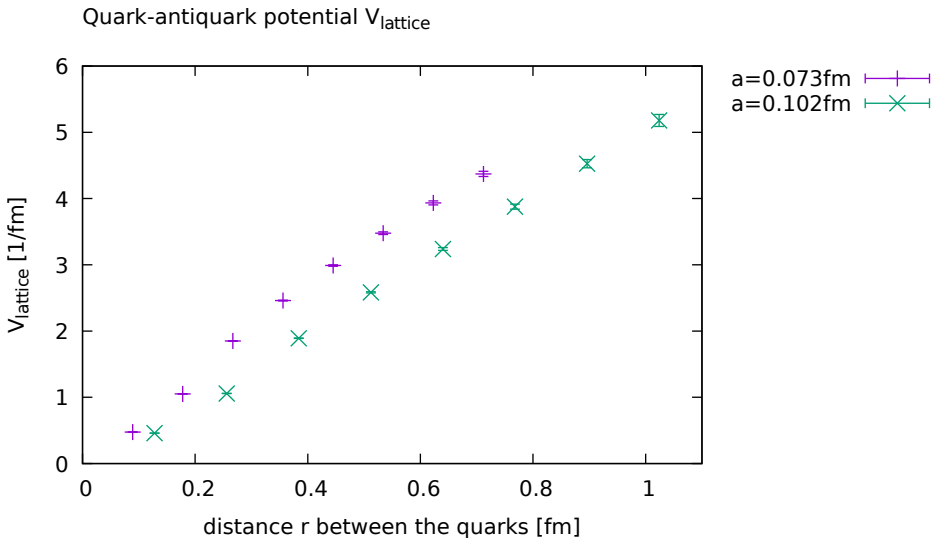

Figure 5.2: Quark antiquark potential $V_{Q\overline{Q}}^{lattice}(r,a)$.
Lattice parameters: $\beta = 2.5 \Rightarrow a = 0.073$ fm and $\beta = 2.4 \Rightarrow a = 0.102$ fm.

Whereas the Coulomb-like part for small distances of quark and antiquark is only vaguely indicated, for both lattice spacings starting from $r \approx 0.4$ fm the linear rise of the potential with the distance of the quarks can be seen. The two slopes of the linear parts (the so called string tension σ) are in agreement, which confirms the expectation that the lattice spacing is chosen small enough to find results corresponding to the limit $a \to 0$. Though the data points for $a = 0.073$ fm are shifted to higher values in comparison to the data points for $a = 0.102$ fm. This is related to the fact that due to Heisenberg's uncertainty relation a smaller lattice spacing corresponds to a wider momentum distribution and therefore also to high momentum contributions. This increases the value of the potential.

The linear rise of the potential characterizes the phenomenon of confinement. Compared to the electric potential, that flattens with increasing distance of the interacting particles and thus produces a decreasing force, the strong force between quark and antiquark is constant irrespective of their distance. Because of this it is to be expected that the gluon field forms a narrow flux tube between the quark and antiquark. This will be investigated in the next chapter.

6 Results: Chromoelectric field

As emphasized in the introduction, the focus of this explanatory study is on the parallel component of the chromoelectric field because its contribution to the energy density is expected to be by far the largest. Taking into account Equation (3.30),

$$\begin{aligned}
&\langle Q\overline{Q},0|\,\mathrm{Tr}\left(\left[E_j(\vec{r}\,')\right]^2\right)|Q\overline{Q},0\rangle - \langle\Omega|\,\mathrm{Tr}\left(\left[E_j(\vec{r}\,')\right]^2\right)|\Omega\rangle \\
&\quad= \lim_{a\to 0}\left\{\langle Q\overline{Q},0|\,\mathrm{Tr}\left(\left[E_j^{lattice}(\vec{r}\,',a/2)\right]^2\right)|Q\overline{Q},0\rangle - \langle\Omega|\,\mathrm{Tr}\left(\left[E_j^{lattice}(\vec{r}\,',a/2)\right]^2\right)|\Omega\rangle\right\} \\
&\quad= \lim_{\substack{\tau\to\infty\\ a\to 0}} \frac{2}{g^2a^4}\left\{\frac{\left\langle W_{C_{L,r,\tau,a}}[U]P_{0j}(\vec{r}\,',\tau/2,a)\right\rangle}{\left\langle W_{C_{L,r,\tau,a}}[U]\right\rangle} - \langle P_{0j}(\vec{r}\,',0,a)\rangle\right\}, \qquad (6.1)
\end{aligned}$$

this means that the spacial direction j of the plaquette has to be chosen in the same direction as the separation axis between quark and antiquark in the calculation of the Wilson loop.

It is important to be be aware of the fact that Equation (6.1) only holds for the limit $a \to 0$. To get an analog of Equation (6.1) on a lattice with finite a, the following two aspects have to be taken into account.

Firstly, a plaquette at spacial lattice point $\vec{r}\,'$ has a non vanishing extension in direction j and therefore yields to a value for the chromoelectric field at point $\vec{r}\,' + \hat{j}/2$ with $\hat{j}$ being a vector in direction j with length a. This is a point between two lattice points. For the limit $a \to 0$, $\vec{r}\,'$ and $\vec{r}\,' + \hat{j}/2$ are identical.

Secondly, the same observation holds for the temporal extension of the plaquette. On a lattice with non vanishing temporal lattice spacing a it is not the starting point of the plaquette but its temporal middle, that has to be located at time $\tau/2$ in the first term of Equation (6.1). This indicates why the temporal extension τ of the Wilson loops in Equation (6.1) should be chosen as an odd multiple of a. Then the starting point of the plaquette can be chosen at time $(\tau - a)/2$ and the end point at time $(\tau + a)/2$ which are both multiples of a and thus temporal points on the lattice.

In consideration of these two remarks, the lattice analog of Equation (6.1) is

$$\begin{aligned}
&\langle Q\overline{Q},0|\,\mathrm{Tr}\left(\left[E_j^{lattice}(\vec{r}\,'+\hat{j}/2,a/2)\right]^2\right)|Q\overline{Q},0\rangle - \langle\Omega|\,\mathrm{Tr}\left(\left[E_j^{lattice}(\vec{r}\,'+\hat{j}/2,a/2)\right]^2\right)|\Omega\rangle \\
&\quad= \lim_{\tau\to\infty} \frac{2}{g^2a^4}\left\{\frac{\left\langle W_{C_{L,r,\tau,a}}[U]P_{0j}(\vec{r}\,',(\tau-a)/2,a)\right\rangle}{\left\langle W_{C_{L,r,\tau,a}}[U]\right\rangle} - \langle P_{0j}(\vec{r}\,',0,a)\rangle\right\}. \qquad (6.2)
\end{aligned}$$

A graphical representation of Equation (6.2) is shown in Figure 6.1.

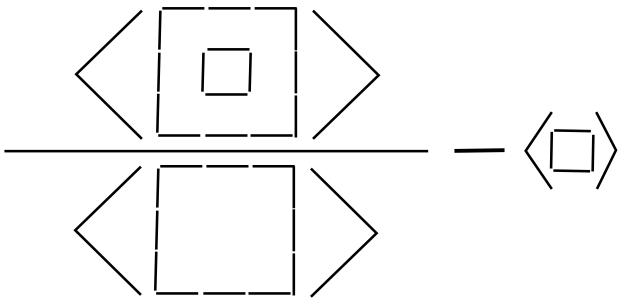

Figure 6.1: Graphical representation of the curly bracket in Equation (6.2).
The figure shows how to evaluate the square of the parallel component of the chromoelectric field generated by a static quark antiquark pair on the lattice.
Extension of the Wilson loop (distance of quark and antiquark): $r = 3a$.
Position, where the chromoelectric field is evaluated: on the quark antiquark axis in the middle between quark and antiquark.

Concretely, in the illustrations below 1/2 times the value of the curly bracket in Equation (6.2) is considered. In order to obtain meaningful absolute values for the chromoelectric field, a renormalisation procedure has to be performed. This is not carried out in this work as it is a challenging project by itself.

For fixed quark antiquark distance r, fixed position $\vec{r}\,'$ of the plaquette related to the quark position $\vec{y}$ and the antiquark position $\vec{x}$ and for fixed τ the right hand side of Equation (6.2) can be evaluated on the lattice in the way described in the following:

The procedure starts with the calculation of the first term. For this purpose, the expectation value of the product of Wilson loop and plaquette and the expectation value of the Wilson loop are calculated separately by averaging over the three possible spacial directions on every lattice point of each configuration. In the product of Wilson loop and plaquette it is necessary to ensure that the temporal and spacial position and the spacial direction of the plaquette is adapted correctly to the position and the direction of the Wilson loop. After the averaging process the quotient between the two expectation values is formed.

For the second term, the value of the plaquette is averaged over the three spacial directions on every lattice point of every configuration.

For both terms the calculated value for every single configuration is saved to generate reduced samples and the jackknife errors from it. Whereas the difference of the two terms is taken to obtain the mean value, the total error is determined by adding up the Jackknife errors of both terms.

In the computation of the Wilson loops APE smearing is used. HYP2 smearing is not used in order to reduce cutoff effects and thereby generate more accurate results near the quarks. The plaquette is computed without using any smearing techniques. This is related to the fact that the correlation between the chromoelectric field and the plaquette was derived for a non-smeared plaquette.

6.1 Temporal extension of the Wilson loop

Firstly, the question arises, which temporal extension of the Wilson loops has to be chosen in order to find results corresponding to the limit $\tau \to \infty$. The best way would be to calculate every lattice quantity for different temporal extensions and observe the behavior with increasing τ as it was done for the potential. If the value of the quantity converges and for some τ reaches a constant value within the measurement error, using this value averaged over some τ starting from the convergence point is reasonable. As this work aims to produce qualitative results and studying the time dependence is quite time-consuming, the time dependence is only investigated exemplary for three lattice quantities. The purpose of this is to decide for a fixed temporal extension of the Wilson loops that yields valid results.

Therefore, the value of the chromoelectric field on three fixed points for different temporal extensions is investigated. Concretely, firstly the spacial extension of the Wilson loop is set to $r = a$ and the plaquette is located on the quark antiquark axis in the spacial middle between quark and antiquark. In doing so, Wilson loop and plaquette have the same spacial extension and position. For the second and third point, $r = 9a$ is used and the plaquette is located on the quark antiquark axis on the first lattice piece next to the quark/antiquark and in the middle between quark and antiquark, respectively.

In the first case presented in Figure 6.2, a clear convergence can be identified. Starting from $\tau \approx 5a$ the value representing the square of the chromoelectric field in parallel direction fluctuates only within the error. The error rises with increasing temporal extension of the Wilson loop, which implies that in order to keep the error small using a small temporal extension is to be preferred. Accordingly, here the choice of $\tau = 5a$ would lead to trustworthy results keeping the error small.

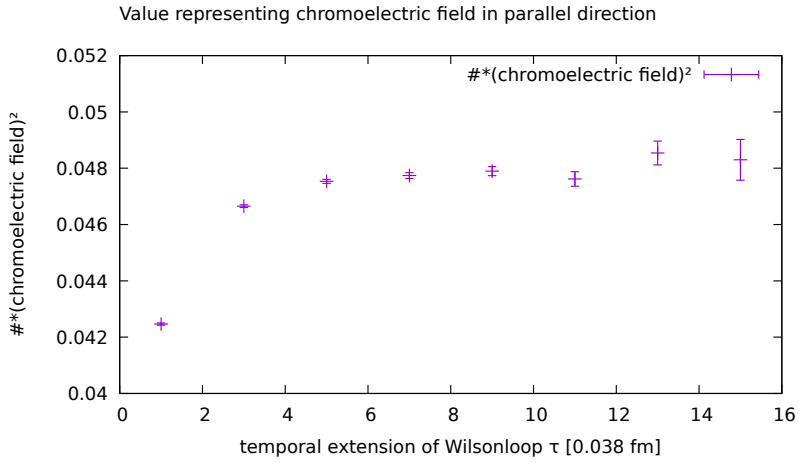

Figure 6.2: Evolution of the value representing the chromoelectric field with rising τ.
1/2 times the value of the curly bracket in Equation (6.2) is plotted.
Lattice parameters: $\beta = 2.7 \Rightarrow a = 0.038$ fm, temporal and spacial extension of the lattice $T = L = 24$, cold start, 20200 configurations produced, of which 200 configurations $\{300, 400, ..., 20200\}$ are used.
APE smearing parameters for the Wilson loops: $N_{APE} = 20$, $\alpha = 0.5$.
Extension of Wilson loop (distance of quark and antiquark): $\boldsymbol{r = 1a}$.
Position, where the chromoelectric field is evaluated: **on the quark antiquark axis in the middle between quark and antiquark**.

In the second case shown in Figure 6.3(a) the value representing the chromoelectric field remains constant within the error for $\tau \in \{1a, 3a, 5a, 7a\}$. For $\tau \geq 9a$ the error increases significantly. This is why the behaviour of the value representing the chromoelectric field in parallel direction for large τ cannot be determined without any doubt. Though, the constant behaviour of the graph for $\tau \in \{1a, 3a, 5a, 7a\}$ indicates that this constant value is a reasonable result. Consequently, the choice of $\tau \in \{1a, 3a, 5a\}$ would make sense to keep the error small.

In the third case in Figure 6.3(b), similar observations as in Figure 6.3(a) can be made. The value remains constant within the error for $\tau \in \{1a, 3a, 5a\}$ and the error increases significantly for $\tau \geq 7a$. As the value is close to zero within error bars, already the result for $\tau = 5a$ has to be treated with caution. Hence, the choice of $\tau \in \{1a, 3a\}$ seems to be appropriate.

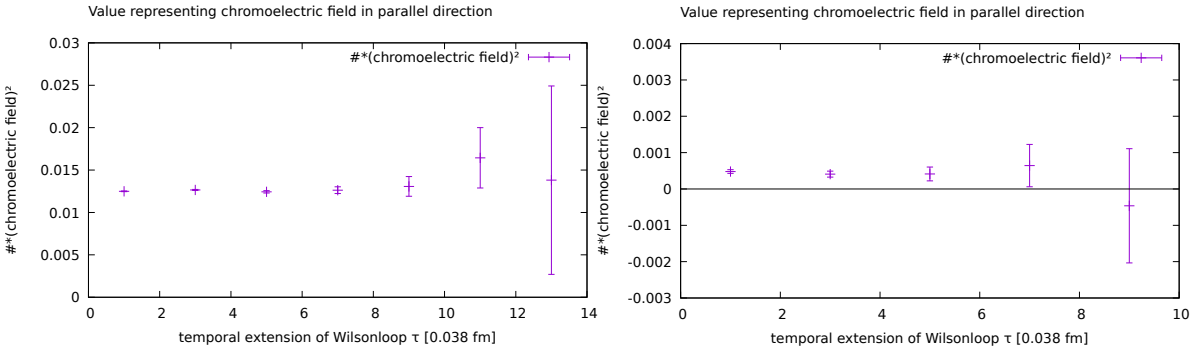

(a) Position, where the chromoelectric field is evaluated:
On the quark antiquark axis in the middle of the first lattice piece next to the quark/antiquark.

(b) Position, where the chromoelectric field is evaluated:
On the quark antiquark axis in the middle between quark and antiquark.

Figure 6.3: Evolution of the value representing the chromoelectric field with rising τ.
1/2 times the value of the curly bracket in Equation (6.2) is plotted.
Lattice parameters: $\beta = 2.7 \Rightarrow a = 0.038$ fm, temporal and spacial extension of the lattice $T = L = 24$, cold start, 20200 configurations produced, of which 200 configurations $\{300, 400, ..., 20200\}$ are used.
APE smearing parameters for the Wilson loops: $N_{APE} = 20$, $\alpha = 0.5$.
Extension of Wilson loop (distance of quark and antiquark): $\boldsymbol{r = 9a}$.

To sum up, the ideal choice of the temporal extension of the Wilson loop to minimize the error and to generate a reasonable result for the chromoelectric field depends on the spacial extension of the Wilson loop and on the position of the plaquette. The choice of $\tau \in \{1a, 3a\}$ produces too low results for small spacial extensions of the Wilson loop and the plaquette in the middle of the quark and antiquark. On the other hand, the choice of $\tau = 5a$ involves errors that are too high to be able to determine the chromoelectric field between quark and antiquark with higher spacial distances in a sufficiently precise way. Accordingly, the following calculations are performed for $\tau = 1a$, $\tau = 3a$ and $\tau = 5a$ keeping in mind the critical aspects of these three choices.

6.2 Chromoelectric field on the quark antiquark axis

In this chapter the chromoelectric field on the quark antiquark axis is evaluated. The spacial extension of the Wilson loop is chosen odd. Therefore, the plaquette can be located either in the middle between quark and antiquark or somewhere else on the quark antiquark axis. If it is not located in the middle, the results at lattice points with same distance to the middle should coincide due to symmetry. This is a useful property as symmetry is a necessary condition and thus a powerful crosscheck of the results. In Figure 6.4 the symmetry of the chromoelectric field within the error bars can be seen.

The property of symmetry can be used to decrease the error by generating only one value for the two symmetry points left and right of the middle. So one averages over twice the number of values, which decreases the jackknife error because also the amount of reduced samples doubles. From now this averaging is applied.

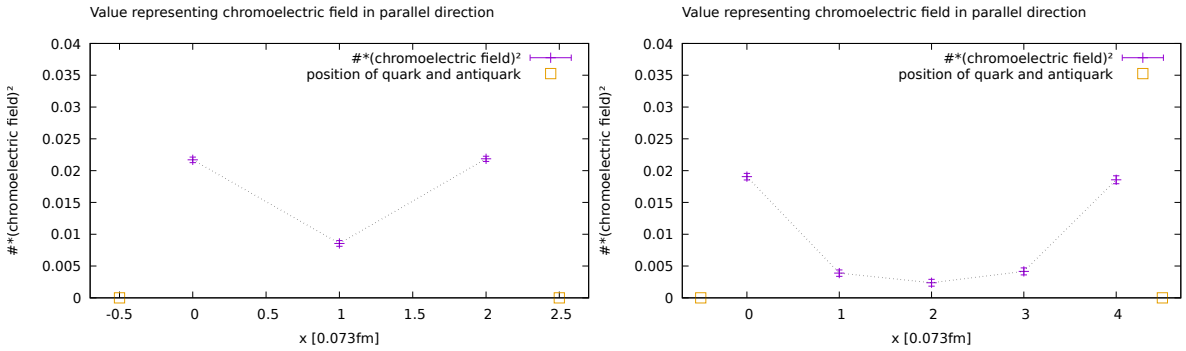

(a) Distance of quark and antiquark $\boldsymbol{r = 3a}$ (b) Distance of quark and antiquark $\boldsymbol{r = 5a}$

Figure 6.4: Symmetry investigation: Lattice value representing the chromoelectric field for two different distances between quark and antiquark.
1/2 times the value of the curly bracket in Equation (6.2) is plotted.
Lattice parameters: $\beta = 2.5 \Rightarrow a = 0.073$ fm, temporal and spacial extension of the lattice $T = L = 18$, hot start, 3200 configurations produced, of which 30 configurations $\{300, 400, ..., 3200\}$ are used.
Temporal extension of the Wilson loops: $\tau = 3a$
APE smearing parameters for the Wilson loops: $N_{APE} = 20$, $\alpha = 0.5$.

In Figure 6.5 and 6.6 the change of the chromoelectric field on the quark antiquark axis with increasing quark antiquark distance is shown. Graphics for $\tau = 1a$ and $\tau = 5a$ are collected. The differences between the two temporal extensions are as discussed in the previous section. Accordingly, for $\tau = 1a$ and small distance of the quark and antiquark (about $r = 1a$ to $r = 5a$) the value for the chromoelectric field in the middle of quark and antiquark is lower than the value for $\tau = 5a$. Also the values for $\tau = 1a$ on other points on the quark antiquark axis slightly differ from the values for $\tau = 5a$ which provide results with smaller systematic error. Thus, for small spatial separations one should use the results for $\tau = 5a$. For bigger spacial distances ($r = 7a$ and $r = 9a$) the value representing the chromoelectric field between the quark and antiquark becomes quite small. In order to be able to distinguish the chromoelectric field from statistic noise, a smaller error is essential so that for bigger spacial distances the choice $\tau = 1a$ is useful.

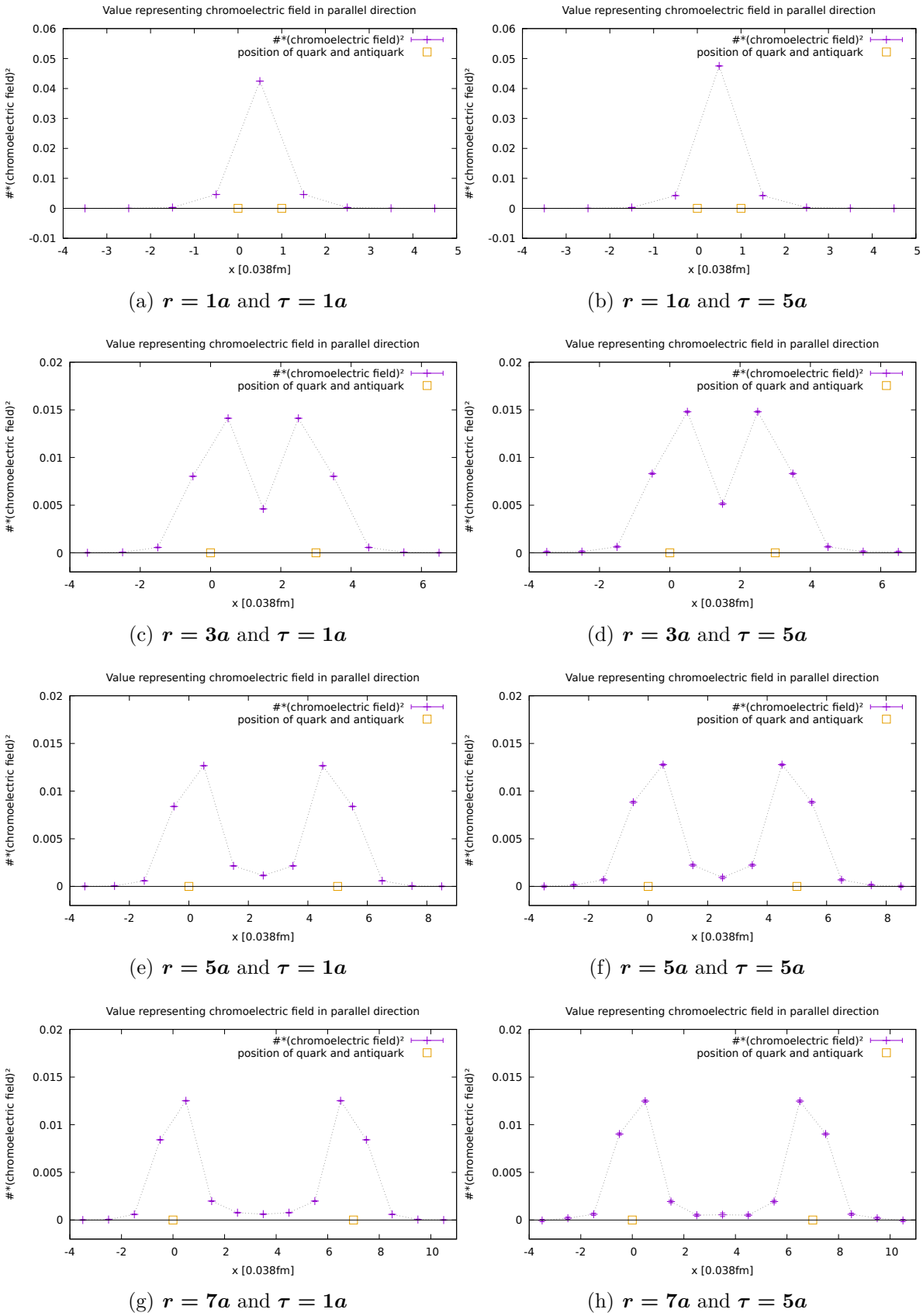

(a) $\boldsymbol{r = 1a}$ and $\boldsymbol{\tau = 1a}$

(b) $\boldsymbol{r = 1a}$ and $\boldsymbol{\tau = 5a}$

(c) $\boldsymbol{r = 3a}$ and $\boldsymbol{\tau = 1a}$

(d) $\boldsymbol{r = 3a}$ and $\boldsymbol{\tau = 5a}$

(e) $\boldsymbol{r = 5a}$ and $\boldsymbol{\tau = 1a}$

(f) $\boldsymbol{r = 5a}$ and $\boldsymbol{\tau = 5a}$

(g) $\boldsymbol{r = 7a}$ and $\boldsymbol{\tau = 1a}$

(h) $\boldsymbol{r = 7a}$ and $\boldsymbol{\tau = 5a}$

Figure 6.5: Chromoelectric field on the quark antiquark axis (1).
1/2 times the value of the curly bracket in Equation (6.2) is plotted.
Lattice parameters: $\beta = 2.7 \Rightarrow a = 0.038$ fm, temporal and spacial extension of the lattice $T = L = 24$, cold start, 20200 configurations produced, of which 200 configurations $\{300, 400, ..., 20200\}$ are used.
APE smearing parameters for the Wilson loops: $N_{APE} = 20$, $\alpha = 0.5$.

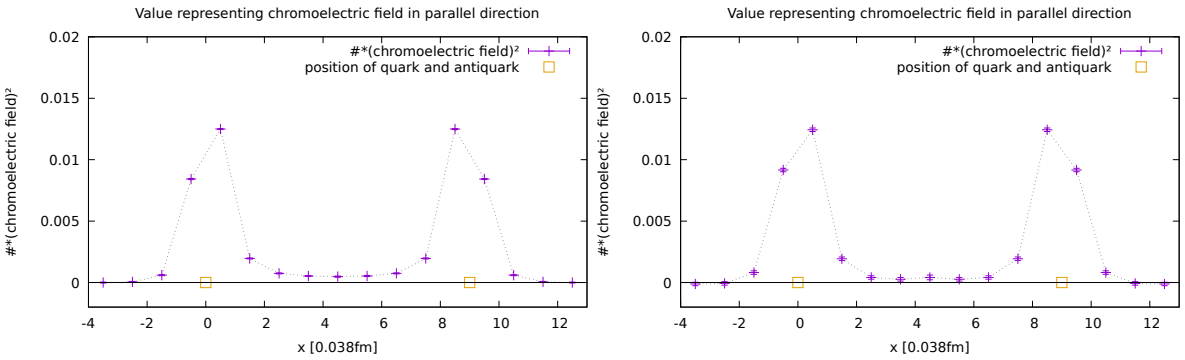

(a) $\boldsymbol{r = 9a}$ and $\boldsymbol{\tau = 1a}$ (b) $\boldsymbol{r = 9a}$ and $\boldsymbol{\tau = 5a}$

Figure 6.6: Chromoelectric field on the quark antiquark axis (2).
1/2 times the value of the curly bracket in Equation (6.2) is plotted.
Lattice parameters: $\beta = 2.7 \Rightarrow a = 0.038$ fm, temporal and spacial extension of the lattice $T = L = 24$, cold start, 20200 configurations produced, of which 200 configurations $\{300, 400, ..., 20200\}$ are used.
APE smearing parameters for the Wilson loops: $N_{APE} = 20$, $\alpha = 0.5$.

As can be seen in Figure 6.5 and 6.6, when quark and antiquark are separated the value of the chromoelectric field between decreases with increasing distance. The value in the middle is the lowest and moving outside towards the quarks it becomes higher and the slope grows.

The plots are in agreement with the phenomenon of confinement. Correspondingly, for bigger spacial distances ($r = 7a$ and $r = 9a$) in the middle of quark and antiquark a region, where the value of the chromoelectric field has a non vanishing constant value within the error, can be observed. It can be excluded that the non vanishing value in the middle is generated by the single quark and antiquark and not by their interaction as on the sides facing away from quark/antiquark the value representing the chromoelectric field drops to zero at a distance of about $3a$ whereas between quark and antiquark a non-vanishing value still remains at a distance of even $4a$.

This already is an indication for the flux tube being formed by pulling apart quark and antiquark. In the next section the cross-sectional area of the flux tube shall be computed by determination of the chromoelectric field beside the quark antiquark axis.

6.3 Chromoelectric field beside the quark antiquark axis

To evaluate the chromoelectric field beside the quark antiquark axis, the position of the plaquette has to be chosen appropriately. In order to keep the symmetry considerations simple, only positions on a two dimensional surface spanned by the quark antiquark axis and one of the two remaining spacial lattice directions perpendicular to this axis are taken into account. Using odd spacial distances between quark and antiquark the plaquette can be located in four different symmetry areas. These are characterised by the number of lattice points that are related by symmetry:

1) The plaquette is located in in the middle between quark and antiquark on the axis, which yields one symmetry value.

2) The plaquette is located on the quark antiquark axis beside the middle, which yields two symmetry values (left/right).

3) The plaquette is located on the axis perpendicular to the quark antiquark axis intersecting the quark antiquark axis in the middle of quark and antiquark, which yields two symmetry values (up/down).

4) The plaquette is located beside these two central axes, which yields four symmetry values (up left, up right, down left, down right).

The four different symmetry areas are shown in Figure 6.7. $\mathrm{pla}_{\mathrm{vertical}}$ gives the distance from the quark antiquark axis in multiples of a.

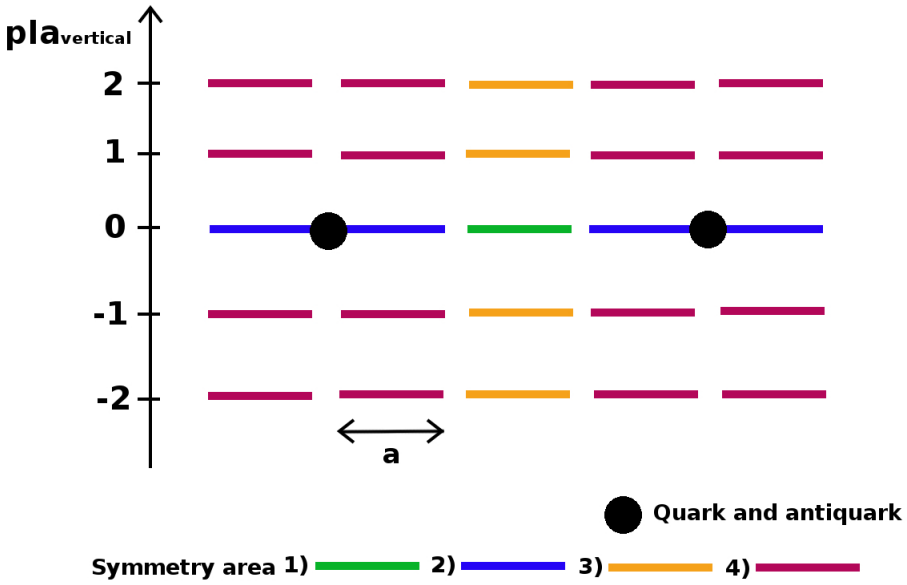

Figure 6.7: Symmetry areas.
The coloured lines show the possible spacial position and extension of the plaquette on a two dimensional spacial surface. The temporal extension of the plaquettes is perpendicular to that surface and cannot be seen in the plot.
Extension of Wilson loop (distance of quark and antiquark): $\boldsymbol{r = 3a}$.

By averaging over all symmetry points (the number of symmetry points depends on the symmetry area), only one value is generated for the one to four symmetry points, that can be assigned to every symmetry point. As in the case on the quark antiquark axis this decreases the error.

Firstly, the profile of the chromoelectric field on axes parallel to the quark antiquark axis is plotted in Figure 6.8. As the distances $r = 5a$ and $r = 9a$ between quark and antiquark are used it can be assumed that the choice $\tau = 1a$ is acceptable.

In the plots on the left hand side the chromoelectric field on the axis ($\text{pla}_{\text{vertical}} = 0$) and for the distances $\text{pla}_{\text{vertical}} \in \{1, 2\}$ is presented whereas on the right hand side it is zoomed into the plot for $\text{pla}_{\text{vertical}} \in \{0, 1, 2, 3\}$ to exhibit the profile of the chromoelectric field beside the quark antiquark axis in detail.

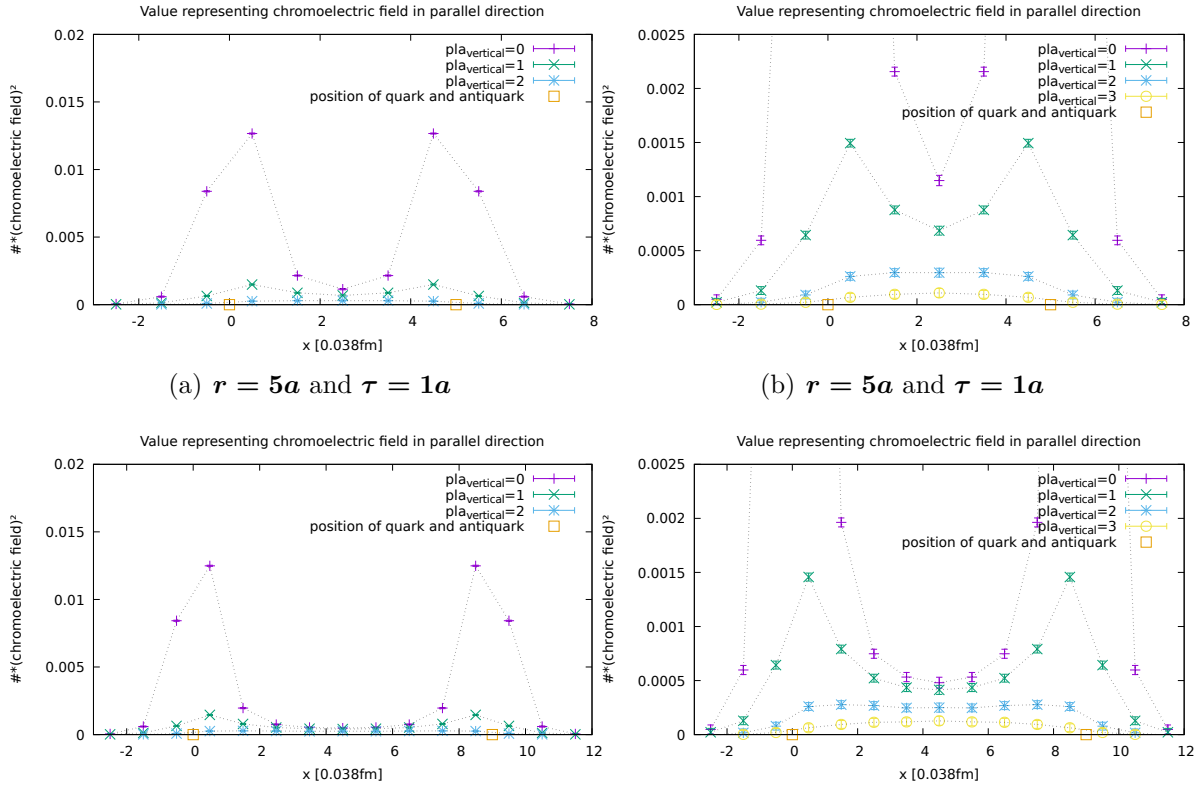

(a) $\boldsymbol{r = 5a}$ and $\boldsymbol{\tau = 1a}$ (b) $\boldsymbol{r = 5a}$ and $\boldsymbol{\tau = 1a}$

(c) $\boldsymbol{r = 9a}$ and $\boldsymbol{\tau = 1a}$ (d) $\boldsymbol{r = 9a}$ and $\boldsymbol{\tau = 1a}$

Figure 6.8: Profiles of the chromolectric field parallel to the quark antiquark axis.
1/2 times the value of the curly bracket in Equation (6.2) is plotted.
Lattice parameters: $\beta = 2.7 \Rightarrow a = 0.038$ fm, temporal and spacial extension of the lattice $T = L = 24$, cold start, 20200 configurations produced, of which 200 configurations $\{300, 400, ..., 20200\}$ are used.
APE smearing parameters for the Wilson loops: $N_{APE} = 20$, $\alpha = 0.5$.

In comparison to the quark antiquark axis the decrease of the chromoelectric field on the axis with $\text{pla}_{\text{vertical}} = 1$ is significant (Figure 6.8(a)/(c)). Nonetheless, for $\text{pla}_{\text{vertical}} = 1$ the peaks at the places where quark and antiquark are located can still be seen clearly in Figure 6.8(b) and (d). Whereas these peaks vanish for $\text{pla}_{\text{vertical}} = 2$ (for $r = 5a$ they vanish completely, for $r = 9a$ signs of these peaks can still be observed) the flux tube, recognizable by the non-vanishing constant value of the chromoelectric field in an area between quark and antiquark, remains even for $\text{pla}_{\text{vertical}} \in \{2, 3\}$. This shows that the flux tube has a relatively large cross-sectional characterised by a diameter of at least 0.2fm. In addition, the profiles for $\text{pla}_{\text{vertical}} = 3$ indicate that the flux tube has a slightly rounded form having the largest radius in the middle between quark and antiquark. The deviation of the flux tube from a straight cylindrical shape can be linked to the $1/r$ correction term providing an additional energy contribution in the formula for the quark antiquark potential [13].

Secondly, the chromoelectric field on the two dimensional surface spanned by the quark antiquark axis and one of the two remaining spacial lattice directions perpendicular to this axis is plotted in Figure 6.9 by using the same values as in Figure 6.8. The colours of the surfaces correspond to the average value of the four chromoelectric field values on the edges of the surface. Whereas the flux tube cannot be seen so well in Figure 6.9(b) for $r = 9a$ as the value of the chromoelectric field in the region of the flux tube is much smaller than the peaks at the places where quark and antiquark are located, the existence of the flux tube in Figure 6.9(a) for $r = 5a$ is clearly visible.

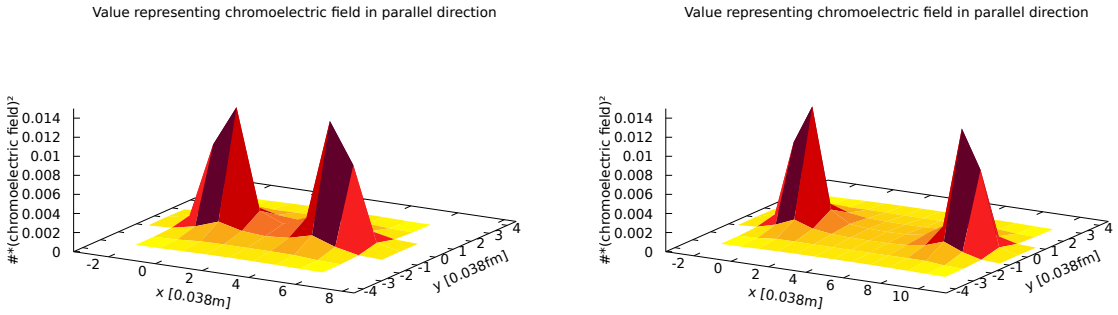

(a) $\boldsymbol{r = 5a}$ and $\boldsymbol{\tau = 1a}$ (b) $\boldsymbol{r = 9a}$ and $\boldsymbol{\tau = 1a}$

Figure 6.9: 3d plots of the chromoelectric field.
1/2 times the value of the curly bracket in Equation (6.2) is plotted.
Lattice parameters: $\beta = 2.7 \Rightarrow a = 0.038$ fm, temporal and spacial extension of the lattice $T = L = 24$, cold start, 20200 configurations produced, of which 200 configurations $\{300, 400, ..., 20200\}$ are used.
APE smearing parameters for the Wilson loops: $N_{APE} = 20$, $\alpha = 0.5$.

7 Conclusion and outlook

In this work the chromoelectric field as a measure of the energy density in the region of an infinitely heavy quark antiquark pair on a two dimensional surface was investigated for different distances of quark and antiquark. Thereby the influence of the temporal extensions of the Wilson loops used in the calculation on the results was studied. In doing so, it has been observed that the chromoelectric field between quark and antiquark has a non vanishing value also for large quark antiquark distances. Moreover, this flux tube has a diameter of at least 0.2fm. These observations are consistent with confinement of the strong interactions.

For further investigations it would be interesting to increase the accuracy of the results by calculating the lattice quantity representing the chromoelectric field on every single lattice point for different temporal extensions and observe the behaviour with increasing τ.

Moreover, a three dimensional analysis of the chromoelectric field taking into account axes parallel to the quark antiquark axis that are not part of the two dimensional surface could deliver results for a larger range of distances from the quark antiquark axis. Consequently, the structure of the flux tube could be investigated more in detail, so that the results can be checked against string model calculations [13].

In order to generate absolute values for the energy density a renormalisation procedure could be performed. A crude but simple way would be to calculate the string tension σ by fitting the potential in Figure 5.2, which gives a value for the increase of energy with increasing quark antiquark distance. Integrating the value representing the square of the parallel chromoelectric field component (and thus also representing the energy density as the other contributions to the energy density are negligibly small) over the whole space around quark and antiquark yields a value for the energy of the quark antiquark binding. In doing so for different quark antiquark distances a value for the string tension σ' is produced, that can be renormalised by assignment to σ, which leads to renormalised energy density values.

Bibliography

[1] P. Cea and L. Cosmai, Nucl. Phys. Proc. Suppl. **47**, 318 (1996) doi:10.1016/0920-5632(96)00065-5 [hep-lat/9509007].

[2] A. Di Giacomo, M. Maggiore and S. Olejnik, Nucl. Phys. B **347**, 441 (1990). doi:10.1016/0550-3213(90)90567-W

[3] P. Bicudo, M. Cardoso and N. Cardoso, PoS LATTICE **2013**, 495 (2014) [arXiv:1401.6008 [hep-lat]].

[4] A. S. Bakry, D. B. Leinweber, P. J. Moran, A. Sternbeck and A. G. Williams, Phys. Rev. D **82**, 094503 (2010) doi:10.1103/PhysRevD.82.094503 [arXiv:1004.0782 [hep-lat]].

[5] A. S. Bakry, D. B. Leinweber and A. G. Williams, Phys. Rev. D **85**, 034504 (2012) doi:10.1103/PhysRevD.85.034504 [arXiv:1011.1380 [hep-lat]].

[6] H. J. Rothe, World Sci. Lect. Notes Phys. **43**, 1 (1992) [World Sci. Lect. Notes Phys. **59**, 1 (1997)] [World Sci. Lect. Notes Phys. **74**, 1 (2005)] [World Sci. Lect. Notes Phys. **82**, 1 (2012)].

[7] S. Lottini, O. Philipsen, M.Wagner. Vorlesungsskript: Quantenfeldtheorie 2 Sommersemester 2013, Version 16.06.2015

[8] M. Wagner. Lattice SU2 program.

[9] O. Philipsen and M. Wagner, Phys. Rev. D **89**, no. 1, 014509 (2014) doi:10.1103/PhysRevD.89.014509 [arXiv:1305.5957 [hep-lat]].

[10] http://www.physics.utah.edu/%7Edetar/phycs6730/handouts/jackknife/jackknife/, date: 31.08.2017

[11] K. Jansen *et al.* [ETM Collaboration], JHEP **0812**, 058 (2008) doi:10.1088/1126-6708/2008/12/058 [arXiv:0810.1843 [hep-lat]].

[12] M. Della Morte, A. Shindler and R. Sommer, JHEP **0508**, 051 (2005) doi:10.1088/1126-6708/2005/08/051 [hep-lat/0506008].

[13] A. M. Green, C. Michael and P. S. Spencer, Phys. Rev. D **55**, 1216 (1997) doi:10.1103/PhysRevD.55.1216 [hep-lat/9610011].